Engineering with Computers (2010) 26:171–183
DOI 10.1007/s00366-009-0155-0

ORIGINAL ARTICLE

The problem of verification with reference to the Girkmann problem

Barna A. Szabó · Ivo Babuška · Juhani Pitkäranta · Sebastian Nervi

Received: 9 July 2009 / Accepted: 10 September 2009 / Published online: 20 November 2009

Abstract This paper is concerned with the problem of verification of the numerical accuracy of computed information with particular reference to a model problem in solid mechanics. The basic concepts and procedures are outlined and illustrated by examples.

Keywords Verification · Reliability · Error estimation · Numerical approximation

1 Introduction

Whenever engineering or scientific computations are performed, there is an implied expectation of reliability. Without this expectation it would not be possible to justify the time, effort and expense involved in performing the computations. For a computation to be justifiable, satisfactory answers have to be given to two questions: (a) What evidence has been provided that the exact solution of the mathematical model is a reasonable representation of the physical reality that it is supposed to represent?, (b) What evidence has been provided that the computed information is sufficiently accurate for the purposes of the decision-making it is expected to serve? This paper is concerned only with the second question, the problem of verification of the numerical accuracy of computed information with specific reference to a model problem in solid mechanics.

The importance of verification is self-evident. Given that most engineering and scientific computations involve numerical approximation, it is not sufficient to report the results. It is necessary also to show that the computed data are within acceptable error tolerances. For example, the editors of the AIAA journals issued the following policy statement [1]:

> *"The AIAA journals will not accept for publication any manuscript reporting (1) numerical solutions of an engineering problem that fails to adequately address the accuracy of the computed results or (2) experimental results unless the accuracy of the data is adequately presented."*

Guidelines for the formulation and numerical treatment of mathematical models for use in support of engineering decision-making in the field of solid mechanics were published by the American Society of Mechanical Engineers (ASME) which were adopted by the American National Standards Institute (ANSI) [2]. A critical discussion of certain aspects of this document is available in [3].

To test how verification procedures would be applied in current professional practice in a specific setting, readers of the bulletin of the International Association for Computational Mechanics, called IACM expressions, were invited to solve the problem described in the following section [4]. The responses received were summarized in a follow-on

B. A. Szabó (✉)
Department of Mechanical, Aerospace and Structural Engineering, Washington University, St. Louis, MO, USA
e-mail: szabo@wustl.edu

I. Babuška
Institute for Computational Engineering and Science, The University of Texas at Austin, Austin, TX, USA

J. Pitkäranta
Institute of Mathematics, Helsinki University of Technology, Helsinki, Finland

S. Nervi
Engineering Software Research and Development, Inc., St. Louis, MO, USA

article [5]. In this paper, a detailed explanation is given of how verification of the accuracy of the data published in [5] was performed.

2 Problem statement

A spherical shell of thickness $h = 0.06$ m, crown radius $R_c = 15.00$ m is connected to a stiffening ring at the meridional angle $\alpha = 2\pi/9$ (40°). The dimensions of the ring are: $a = 0.60$ m, $b = 0.50$ m. The radius of the mid-surface of the spherical shell is $R_m = R_c / \sin\alpha$. The notation is shown in Fig. 1. The z axis is the axis of rotational symmetry.

The shell is made of reinforced concrete, assumed to be homogeneous, isotropic and linearly elastic with Young's modulus $E = 20.59$ GPa and Poisson's ratio $\nu = 0$.

Consider gravity loading only. The equivalent (homogenized) unit weight of the material comprised of the shell and the cladding is 32.69 kN/m^3. Assume that uniform normal pressure p_{AB} is acting at the base AB of the stiffening ring. The resultant of p_{AB} equals the weight of the structure. Assume that the stiffening ring is weightless. The goals of computation are as follows:

1. Find the shearing force Q_α in kN/m units and the bending moment M_α in Nm/m units acting at the junction between the spherical shell and the stiffening ring.
2. Determine the location (meridional angle) and the magnitude of the maximum bending moment in the shell.
3. Verify that the results are accurate to within 5%.

This problem was first discussed by Girkmann [6], subsequently by Timoshenko and Woinowski-Krieger [7]. Solutions by classical methods are presented in both references. The stiffening ring was assumed to be weightless.

Remark 1 The foregoing problem statement differs from the original problem statement by Girkmann in two respects: In [6], kgf (resp. cm) was used for the unit of force (resp. length). In [7], lbf and inch units were used. Here we use SI units. Also, one of the goals of computation was to determine the radial force per unit length between the ring and the shell. Here the goal is to determine the shear force per unit length between the ring and the shell.

Remark 2 Since the problem is statically determinate with respect to forces acting in the axial direction, the pressure acting on the base of the ring AB can be computed from the information provided. If the ring is assumed to be weightless then the uniformly distributed pressure acting on the base of the ring is $p_{AB} = 27.256$ kPa. If the ring is assumed to have the same unit weight as the shell then $p_{AB} = 43.553$ kPa.

Remark 3 According to the problem statement the shell is made of reinforced concrete, yet it is assumed to be homogeneous and isotropic. While the two statements are contradictory, this is a commonly used idealization in civil engineering practice. The inhomogeneity and anisotropy caused by the reinforcement are neglected. We emphasize that in this paper we are not concerned with the question of whether the mathematical problem formulated in the

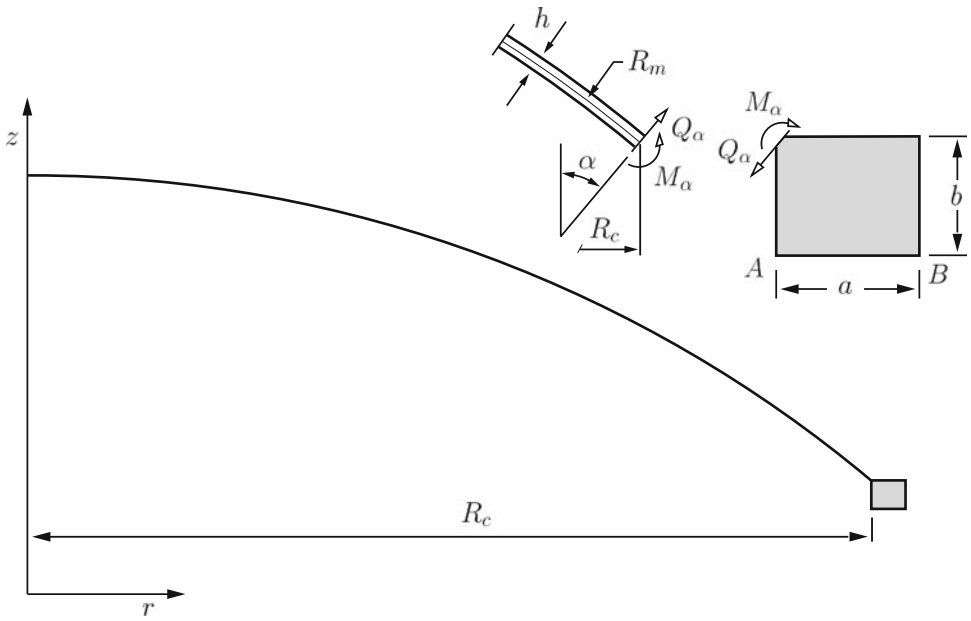

Fig. 1 The Girkmann problem. Notation

following section is a realistic model of a spherical shell stiffened by a footring; clearly it is not. We are concerned only with verification of the numerical solution of the problem.

3 Formulation of the mathematical problem

We understand the Girkmann problem as a problem of three-dimensional (3D) elasticity on the domain of a spherical shell, stiffened by a ring. Because the domain, the material properties and the boundary conditions are axially symmetric, we will formulate the problem taking advantage of simplifications made possible by the a priori information that in cylindrical coordinates r, θ, z the solution is independent of the angle θ.

The elastostatic equations of equilibrium for axially symmetric problems in cylindrical coordinates are [8]:

$$\frac{1}{r}\frac{\partial(r\sigma_r)}{\partial r}+\frac{\partial\tau_{rz}}{\partial z}-\frac{\sigma_\theta}{r}+F_r=0 \tag{1}$$

$$\frac{1}{r}\frac{\partial(r\tau_{rz})}{\partial r}+\frac{\partial\sigma_z}{\partial z}+F_z=0 \tag{2}$$

where z is the axis of rotational symmetry and r is the radial coordinate, as shown in Fig. 1. The terms F_r and F_z represent the components of the volume forces in the radial and axial directions, respectively.

On multiplying Eq. (1) by a test function $v_r = v_r(r, z)$ and Eq. (2) by a test function $v_z = v_z(r, z)$, integrating over the volume of the axially symmetric body and applying the divergence theorem, we have the statement of the principle of virtual work for axially symmetric elastostatic problems:

$$\int_\Omega\left(\sigma_r\frac{\partial v_r}{\partial r}+\sigma_\theta\frac{v_r}{r}+\sigma_z\frac{\partial v_z}{\partial z}+\tau_{rz}\left(\frac{\partial v_r}{\partial z}+\frac{\partial v_z}{\partial r}\right)\right)r\mathrm{d}r\mathrm{d}z = \int_\Omega(F_rv_r+F_zv_z)r\mathrm{d}r\mathrm{d}z+\int_\Gamma(T_rv_r+T_zv_z)r\mathrm{d}s \tag{3}$$

where Ω is the domain of the generating surface and Γ is the boundary of Ω, T_r and T_z represent the surface tractions. By definition:

$$T_r=\sigma_rn_r+\tau_{rz}n_z \tag{4}$$

$$T_z=\tau_{rz}n_r+\sigma_zn_z \tag{5}$$

where n_r, n_z are the components of the unit normal to Γ. Because v_r and v_z are arbitrary, Eq. (3) holds for all $\mathbf{v}=\{v_r\ \ v_z\}^T$ for which the indicated operations are defined. Vector $\mathbf{v}$ is called the virtual displacement vector. The displacement vector will be denoted by $\mathbf{u}=\{u_r\ \ u_z\}^T$.

We denote the Lamé parameters by λ and G and define the operator matrix $\mathbf{D}$ and the material stiffness matrix $\mathbf{E}$ as follows:

$$\mathbf{D}=\begin{bmatrix}\partial/\partial r & 0\\ 1/r & 0\\ 0 & \partial/\partial z\\ \partial/\partial z & \partial/\partial r\end{bmatrix},$$

$$\mathbf{E}=\begin{bmatrix}\lambda+2G & \lambda & \lambda & 0\\ \lambda & \lambda+2G & \lambda & 0\\ \lambda & \lambda & \lambda+2G & 0\\ 0 & 0 & 0 & G\end{bmatrix}. \tag{6}$$

We denote the strain vector by $\epsilon=\{\epsilon_r\ \epsilon_\theta\ \epsilon_z\ \gamma_{rz}\}^T$. Using the definition of strain in axially symmetric problems (see for example [8]), we have $\epsilon=\mathbf{Du}$. Using Hooke's law we have $\boldsymbol{\sigma}=\mathbf{E}\epsilon=\mathbf{EDu}$ where $\boldsymbol{\sigma}=\{\sigma_r\ \sigma_\theta\ \sigma_z\ \tau_{rz}\}^T$ is the stress vector. We define:

$$B_\Omega(\mathbf{u},\mathbf{v})=\int_\Omega(\mathbf{Dv})^T\mathbf{EDu}r\mathrm{d}r\mathrm{d}z \tag{7}$$

$$F_\Omega(\mathbf{v})=\int_\Omega(F_rv_r+F_zv_z)r\mathrm{d}r\mathrm{d}z+\int_\Gamma(T_rv_r+T_zv_z)r\mathrm{d}s. \tag{8}$$

In engineering terminology $\mathbf{v}$ is the virtual displacement field, $B_\Omega(\mathbf{u}, \mathbf{v})$ is the virtual work of internal stresses and $F_\Omega(\mathbf{v})$ is the virtual work of external forces. Next we define the energy space $E(\Omega)$:

$$E(\Omega)=\{\mathbf{u}|B_\Omega(\mathbf{u},\mathbf{u})<\infty\}. \tag{9}$$

We associate the energy norm with $E(\Omega)$:

$$\|\mathbf{u}\|_{E(\Omega)}=\left(\frac{1}{2}B_\Omega(\mathbf{u},\mathbf{u})\right)^{1/2}. \tag{10}$$

We denote the domain occupied by the generating section of the spherical shell by Ω_S and the domain occupied by the generating section of the ring by Ω_R. Therefore $\Omega=\Omega_S\cup\Omega_R$.

In the Girkmann problem, the ring is assumed to be weightless. Therefore $F_r=0$ on Ω, $F_z=-32.69$ kN/m^3 on Ω_S, $F_z=0$ on Ω_R, $T_r=0$ on Γ, $T_z=27.256$ kPa on Γ_{AB} (see Remark 2) and $T_z=0$ on $\Gamma-\Gamma_{AB}$ where Γ_{AB} is the base of the ring, represented by the boundary segment AB in Fig. 1. The mathematical problem is to find $\mathbf{u_{EX}}\in E(\Omega)$ such that

$$B_\Omega(\mathbf{u_{EX}},\mathbf{v})=F_\Omega(\mathbf{v})\quad\text{for all }\mathbf{v}\in E(\Omega) \tag{11}$$

and, having found $\mathbf{u_{EX}}$, determine the data of interest specified in the problem statement.

The boundary conditions are prescribed tractions that satisfy equilibrium. Therefore $\mathbf{u_{EX}}$ exists in $E(\Omega)$ and it is unique up to rigid body displacement in the direction of the z axis. There are various ways by which a rigid body constraint can be imposed. For example the average

displacement of the base of the ring (line AB in Fig. 1) can be set to zero or some other fixed value. In finite element analysis u_z is typically set to zero in an arbitrary node. The energy space subject to rigid body constraint will be denoted by $E^0(\Omega)$. Enforcement of the rigid body constraint does not affect of the data of interest.

Remark 4 We will also consider a variant of this problem where the ring has the same unit weight as the shell. In that case $F_r = 0$ on Ω, $F_z = -32.69$ kN/m^3 on Ω, $T_r = 0$ on Γ, $T_z = 43.553$ kPa on Γ_{AB} and $T_z = 0$ on $\Gamma - \Gamma_{AB}$.

4 Approximation

The exact solution of the problem formulated in Sect. 3 is not known. To make the problem tractable by classical methods or by numerical means, some method of discretization has to be used for finding an approximation to the exact solution. This means that a subspace of $E(\Omega)$ has to be constructed and an approximate solution sought in the subspace. Of course, the approximate solution will depend on the choice of the subspace. It is understood, however, that the approximate solution is an approximation to $\mathbf{u_{EX}}$ defined by Eq. (11). In the following discretizations used in classical and finite element analyses are briefly described.

4.1 Classical analyses

In classical analyses, such as those presented in [6, 7], kinematic assumptions (also called dimensional reduction or semi-discretization) are used. The shell is formulated in spherical coordinates ϱ, θ, φ called, respectively, the radial coordinate, circumferential angle (longitude) and the meridional angle (colatitude). In axially symmetric problems, such as the Girkmann problem, the solution is independent of θ. Therefore the displacement vector has only two components; u_φ and u_ϱ. We mention two schemes of dimensional reduction specialized for spherical shells subject to axisymmetric conditions.

The Naghdi shell model [9], restricted to the axisymmetric case, is based on the following kinematic assumptions:

$$u_\varphi = u_0(\varphi) + (\varrho - R_\mathrm{m})\psi(\varphi), \quad u_\varrho(\varphi) = w(\varphi) \tag{12}$$

where φ and ϱ are spherical coordinates. The displacement field is characterized by three 1D field functions: $u_0(\varphi)$ (resp. $w(\varphi)$) is the displacement of the mid-surface in the tangential (resp. normal) direction, $\psi(\theta)$ is the angular rotation of the normal to the mid-surface.

The Novoshilov shell model [10], restricted to the axisymmetric case, is based on the following kinematic assumptions:

$$u_\varphi = u_0(\varphi) + \frac{(\varrho - R_\mathrm{m})}{R_\mathrm{m}}\left(u_0(\varphi) - \frac{\mathrm{d}w}{\mathrm{d}\varphi}\right), \; u_\varrho(\varphi) = w(\varphi). \tag{13}$$

In this case the, displacement field is characterized by the displacement components of the mid-surface in the tangential and normal directions, denoted by $u_0(\varphi)$ and $w(\varphi)$, respectively. The shear strain $\gamma_{\varphi\varrho}$ corresponding to this displacement field is zero. This restriction is known as the Kirchhoff–Love constraint which is often stated as the assumption that normals to the mid-surface of the shell in the reference configuration remain normals in the deformed configuration. In references [6, 7], the Novoshilov shell model was used. Additional assumptions were introduced concerning the ring: It was assumed that the ring can be treated as if it had a rectangular cross section and the deformation of the ring can be characterized by two numbers, the radial displacement of the centroid and the angle of rotation with respect to the centroid. A detailed analysis of this and similar assumptions is available in [11].

Remark 5 There is a large literature on the formulation and justification of linear and nonlinear shell models. See, for example [12, 13]. The intent is to approximate the solution of the problem of 3D elasticity by a problem made simpler through the introduction of kinematic assumptions such as those in Eqs. (12) and (13). The justification of these models is based on asymptotic analysis: A shell model is formulated such that its exact solution is the correct limit of the exact solution of the model based on 3D linear or nonlinear elasticity when the thickness of the shell approaches zero. Implied is the assumption that when the thickness is sufficiently small then the exact solution of the shell model will be a close representation of the exact solution of the 3D model. We will understand here that the goal is to approximate the exact solution of the 3D problem of linear elasticity, not the solution of a particular shell model.

4.2 Finite element analysis

We first consider finite element approximation of the solution of the problem given by Eq. (11). We define a finite dimensional subspace $S^0(\Omega)$ of $E^0(\Omega)$. The subspace $S^0(\Omega)$ is characterized by the finite element mesh, comprised of triangular and/or quadrilateral elements, the polynomial degrees assigned to the elements and the functions that map the standard triangular or quadrilateral element onto the elements of the mesh. The data presented in this paper were computed with StressCheck[1]. In StressCheck the mapping

[1] StressCheck is a trademark of Engineering Software Research and Development, Inc., St. Louis, Missouri, USA.

functions are based on the blending function method. Curved boundaries and surfaces are approximated by polynomial functions using optimal collocation points. For details we refer to [14–16]. The dimension of $S^0(\Omega)$ is the number of degrees of freedom (*df*), denoted by *N*.

The finite element solution $\mathbf{u_{FE}}$ is that function in $S^0(\Omega)$ which satisfies the condition:

$$B_\Omega(\mathbf{u_{FE}}, \mathbf{v}) = F_\Omega(\mathbf{v}) \quad \text{for all } \mathbf{v} \in S^0(\Omega). \tag{14}$$

An important property of the finite element solution is that it is the best approximation to the exact solution $\mathbf{u_{EX}}$ in energy norm, given the space $S^0(\Omega)$:

$$\|\mathbf{u_{EX}} - \mathbf{u_{FE}}\|_{E(\Omega)} = \min_{\mathbf{u}\in S^0(\Omega)} \|\mathbf{u_{EX}} - \mathbf{u}\|_{E(\Omega)}. \tag{15}$$

For additional details and proof we refer (for example) to [14]. This statement shows that the error of approximation, measured in energy norm, depends on the choice of $S^0(\Omega)$. Furthermore, if we construct a sequence of finite element spaces such that $S_1^0(\Omega) \subset S_2^0(\Omega), \ldots, S_n^0(\Omega)$ and compute the corresponding finite element solutions $\mathbf{u_{FE}}^{(1)}$, $\mathbf{u_{FE}}^{(2)}$,..., $\mathbf{u_{FE}}^{(n)}$ then the error $\|\mathbf{u_{EX}} - \mathbf{u_{FE}}^{(k)}\|_{E(\Omega)}$ decreases monotonically with respect to increasing *k*.

5 Extraction and error estimation

Since the exact solution of this problem is not known, the error in the numerical solution has to be estimated. It is possible to obtain guaranteed upper and lower bounds of the error in the data of interest [17, 18], however, owing to the complexity of the procedure, in engineering practice this is not feasible.

In practice one of the most general and robust methods used for estimating the errors of approximation is to compute solutions corresponding to a converging sequence of discretizations. Although this approach will not give guaranteed error bounds, it is very reliable. Since the exact solution is independent of the discretization, a necessary condition for the errors in the data of interest to be small is that the data of interest are substantially independent of the discretization. To make the stronger statement that the errors in the data of interest are within a given tolerance involves extrapolation and judgment that the extrapolated values are sufficiently close to their exact counterparts to justify making the statement. This method of error estimation is based on the assumptions that (a) the data of interest are finite numbers and (b) convergence of the sequence of discretizations in energy norm has been proven. The accuracy of the solution in energy norm is an important measure of the quality of the approximate solution. Although good accuracy in energy norm is not always necessary for ensuring that errors in the data of interest are small, it should always be taken into consideration.

We are interested in computing the location and magnitude of the maximum bending moment $M_{\max}$ and the bending moment M_α and the shear force Q_α at the interface between the shell and the ring. Referring to Fig. 2a, point P_0 indicates the intersection between the mid-surface of the shell and the ring at $\varphi = \alpha$. We denote the coordinates of P_0 by (R_c, Z_c). The coordinates of an arbitrary point P on the interface are denoted by (r, z).

By definition:

$$M_\varphi = \frac{1}{R_c} \int_{-h/2}^{h/2} (T_z(r - R_c) - T_r(z - Z_c)) r \mathrm{d}s \tag{16}$$

$$Q_\varphi = \frac{1}{R_c} \int_{-h/2}^{h/2} (T_r \sin\varphi + T_z \cos\varphi) r \mathrm{d}s. \tag{17}$$

Writing

$$r - R_c = s\sin\varphi, \quad z - Z_c = s\cos\varphi \tag{18}$$

and

$$T_n = T_r \cos\varphi - T_z \sin\varphi, \quad T_s = T_r \sin\varphi + T_z \cos\varphi \tag{19}$$

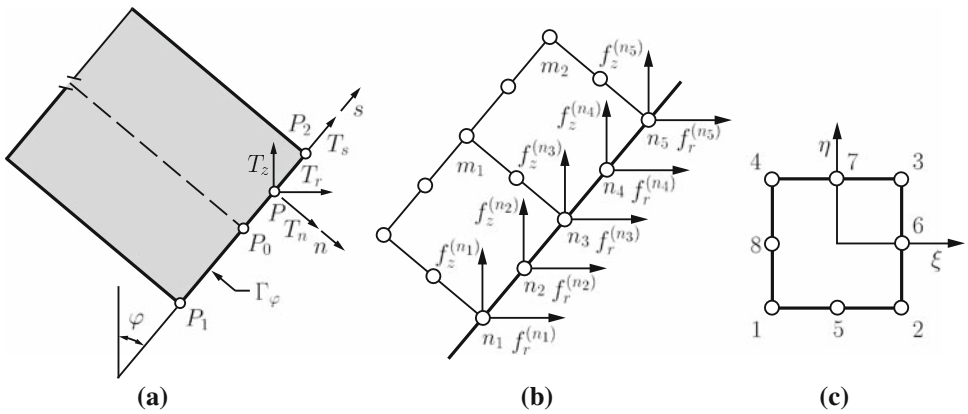

Fig. 2 Notation

we have

$$M_\varphi = -\frac{1}{R_c}\int_{-h/2}^{h/2} T_n s r \mathrm{d}s, \quad Q_\varphi = \frac{1}{R_c}\int_{-h/2}^{h/2} T_s r \mathrm{d}s. \tag{20}$$

5.1 Computation of M_α and Q_α by extraction

The procedures for computing the moment M_α and the shear force Q_α at the shell–ring interface from the finite element solution $\mathbf{u_{FE}}$ are outlined in the following. These procedures are based on the ideas presented in [19]. We retain the definitions given by Eqs. (7)–(10), however, we replace Ω with Ω_S.

Let us assume for the moment that the exact solution $\mathbf{u_{EX}}$ on the entire domain Ω is known. We define an extraction function $\mathbf{w}^{(\mathbf{M})} \in E(\Omega_S)$ subject to the kinematic boundary conditions: $w_n^{(M)} = -s$, $w_s^{(M)} = 0$ on Γ_α and apply the principle of virtual work on Ω_S:

$$B_{\Omega_S}(\mathbf{u_{EX}}, \mathbf{w}^{(\mathbf{M})}) = \int_{\Omega_S} F_z w_z^{(M)} r \mathrm{d}r\mathrm{d}z - \underbrace{\int_{\Gamma_\alpha} T_n s r \mathrm{d}s}_{R_c M_\alpha^{(EX)}}.$$

Therefore

$$M_\alpha^{(\mathrm{EX})} = \frac{1}{R_c}\left(B_{\Omega_S}(\mathbf{u_{EX}}, \mathbf{w}^{(\mathbf{M})}) - \int_{\Omega_S} F_z w_z^{(M)} r \mathrm{d}r\mathrm{d}z \right). \tag{21}$$

If we now replace $\mathbf{u_{EX}}$ with $\mathbf{u_{FE}}$, we have:

$$M_\alpha^{(\mathrm{FE})} = \frac{1}{R_c}\left(B_{\Omega_S}(\mathbf{u_{FE}}, \mathbf{w}^{(\mathbf{M})}) - \int_{\Omega_S} F_z w_z^{(M)} r \mathrm{d}r\mathrm{d}z \right). \tag{22}$$

On subtracting Eq. (22) from Eq. (21), we have the error in M_α:

$$M_\alpha^{(\mathrm{EX})} - M_\alpha^{(\mathrm{FE})} = \frac{1}{R_c} B_{\Omega_S}(\mathbf{u_{EX}} - \mathbf{u_{FE}}, \mathbf{w}^{(\mathbf{M})}) \tag{23}$$

on applying the Schwarz inequality we have

$$|M_\alpha^{(\mathrm{EX})} - M_\alpha^{(\mathrm{FE})}| \le \frac{2}{R_c} \|\mathbf{u_{EX}} - \mathbf{u_{FE}}\|_{E(\Omega_S)} \|\mathbf{w}^{(\mathbf{M})}\|_{E(\Omega_S)} \tag{24}$$

where the mutiplier 2 comes from our definition of the energy norm, see Eq. (10). This estimate shows that $M_\alpha^{(\mathrm{FE})}$ will converge to $M_\alpha^{(\mathrm{EX})}$ at least as fast as $\mathbf{u_{FE}}$ converges to $\mathbf{u_{EX}}$ in energy norm. It is possible to improve this estimate and show that

$$|M_\alpha^{(\mathrm{EX})} - M_\alpha^{(\mathrm{FE})}| \le \frac{2}{R_c} \|\mathbf{u_{EX}} - \mathbf{u_{FE}}\|_{E(\Omega)} \|\mathbf{z}_{\mathbf{EX}}^{(\mathbf{M})} - \mathbf{z}_{\mathbf{FE}}^{(\mathbf{M})}\|_{E(\Omega)} \tag{25}$$

where $\mathbf{z}_{\mathbf{EX}}^{(\mathbf{M})}$ is a smooth auxiliary function uniquely defined by the extraction function $\mathbf{w}^{(\mathbf{M})}$. This inequality indicates that the error in M_α, more generally the error in any data of interest computed by extraction, can converge to zero faster than the error in energy norm, depending on the smoothness of $\mathbf{z}_{\mathbf{EX}}^{(\mathbf{M})}$ and the sequence of discretizations. The proof of inequality (25) is presented in the Appendix.

The construction of the extraction function for Q_α, denoted by $\mathbf{w}^{(\mathbf{Q})}$, is analogous. The essential boundary conditions on $\mathbf{w}^{(\mathbf{Q})}$ are: $w_n^{(Q)} = 0$, $w_s^{(Q)} = 1$ on Γ_α.

The computation can be simplified if we select $\mathbf{w}^{(\mathbf{M})}$ such that it is zero over all but a few elements in the neighborhood of Γ_α. We define

$$\begin{aligned}\Omega_S^{\alpha,\beta} &= \{r, z | r = \varrho \sin\varphi,\ z \\ &= \varrho\cos\varphi,\ R_m - h/2 < \varrho < R_m + h/2,\ \beta < \varphi < \alpha\}\end{aligned} \tag{26}$$

where R_m is the radius of the mid-surface of the shell and β is a meridional angle corresponding to an element boundary. In the following example we will use $\beta = 35°$, see Fig. 3. Let

$$\begin{aligned}S_M(\Omega_S^{\alpha,\beta}) = \{\mathbf{u} | \mathbf{u} \in E(\Omega_S^{\alpha,\beta}),\ u_n = -s,\ u_s = 0 \text{ on } \Gamma_\alpha, \\ u_n = u_s = 0 \text{ on } \Gamma_\beta\}\end{aligned} \tag{27}$$

and

$$\begin{aligned}S_M^0(\Omega_S^{\alpha,\beta}) = \{\mathbf{u} | \mathbf{u} \in E(\Omega_S^{\alpha,\beta}),\ u_n = u_s = 0 \text{ on } \Gamma_\alpha, \\ u_n = u_s = 0 \text{ on } \Gamma_\beta\}.\end{aligned} \tag{28}$$

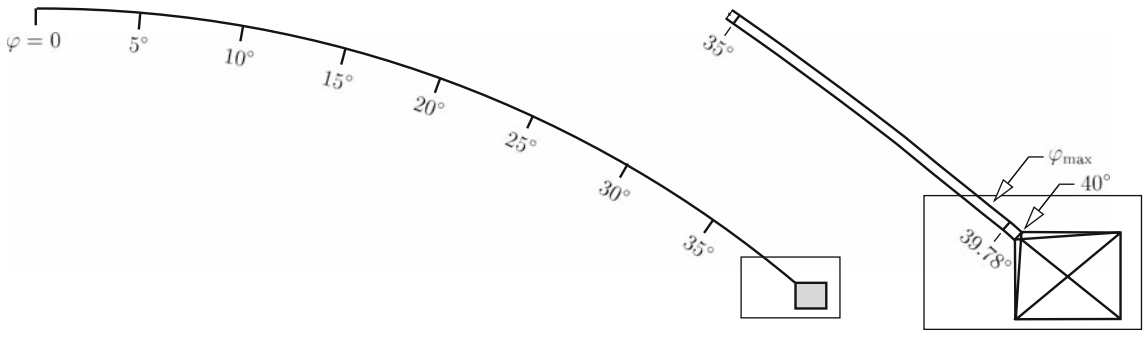

Fig. 3 The 16-element mesh. The location of the maximum bending moment is indicated by $\varphi_{\max}$

We define $\mathbf{w}^{(\mathbf{M})}$ such that $\mathbf{w}^{(\mathbf{M})} \in S_M(\Omega_S^{\alpha,\beta})$ and

$$\int_{\Omega_S^{\alpha,\beta}} (\mathbf{Dv})^T \mathbf{E} \mathbf{D} \mathbf{w}^{(M)} r \mathrm{d}r \mathrm{d}z = 0 \quad \text{for all } \mathbf{v} \in S_M^0(\Omega_S^{\alpha,\beta}). \tag{29}$$

This definition of $\mathbf{w}^{(\mathbf{M})}$ is advantageous from the computational point of view because the term $B_{\Omega_S^{\alpha,\beta}}(\mathbf{u_{FE}}, \mathbf{w}^{(\mathbf{M})})$ can be evaluated by multiplying the stiffness matrices of those elements that lie in $\Omega_S^{\alpha,\beta}$ with the coefficients of the corresponding solution vectors and the transpose of the coefficients of the basis functions corresponding to $\mathbf{w}^{(\mathbf{M})}$. Similarly, evaluation of the second term in the appropriately modified Eq. (22) involves multiplication of the load vectors with the coefficients that characterize $\mathbf{w}^{(\mathbf{M})}$. The definition of $\mathbf{w}^{(\mathbf{Q})}$ is analogous.

For example, using the mesh shown in Fig. 3 and $\beta = 35°$ the functions $\mathbf{w}^{(\mathbf{M})}$ and $\mathbf{w}^{(\mathbf{Q})}$ are shown in Fig. 4. Using these extraction functions we find $M_\alpha = -36.81$ Nm/m and $Q_\alpha = 943.6$ N/m when $p = 8$. The trunk space was used for the computation of $\mathbf{u_{FE}}$ and the extraction functions.

Remark 6 The length of the small element bounded by the radial lines at $\varphi = 39.78°$ and $\varphi = 40°$, shown in Fig. 3, is 1.5 times the thickness of the shell. Such elements are commonly used in plate and shell problems approximated by the p-version in order to provide good approximation properties at the boundary layer. We will refer to this element as the boundary layer element.

It is interesting to note that if we did not have the boundary layer element, that is, the length of all elements that cover the shell were the same (5°) and therefore the mesh consisted of 15 elements only, then the extracted values of the stress resultants would be $M_\alpha = -36.91$ Nm/m, which differs from the previously obtained result by less than 0.3% and Q_α would remain the same.

Remark 7 The curved boundaries were approximated by a collocation scheme based on [16], using six collocation points. In other words polynomials of degree 5 were used for approximating the curved boundaries of the elements. This is the default value in StressCheck, which is fixed independent of the polynomial degree used in the approximation. Mapping was performed by the blending function method.

The quality of the mapping was tested using the following measure:

$$d = 100 \left| (R_\mathrm{m} \pm h/2) - \sqrt{r^2 + z^2} \right| / h \tag{30}$$

where R_m is the mean radius of the shell, h is the thickness, r and z are coordinates of the mapped surface. Measure d is the difference between the radius of the ideal sphere and the mapped radius, expressed as a percentage of the thickness of the shell. For both the outer and inner surfaces the maximum value of d was approximately 1.6×10^{-8}, therefore the mapping error is negligibly small. This error has a periodic character because the elements have the same length, with the exception of the two elements near the interface with the ring. The mapping error was smaller for these elements.

5.2 Computation of Q_α and M_α from nodal forces

Stress resultants are typically computed from nodal forces in h-version codes. We will show that this is formally identical to the method described in Sect. 1, however, the extraction function is mesh-dependent and therefore one cannot speak of convergence of the auxiliary functions $\|\mathbf{z}_{\mathbf{EX}}^{(\mathbf{M})} - \mathbf{z}_{\mathbf{FE}}^{(\mathbf{M})}\|_{E(\Omega_S)}$ in Eq. (25). Nodal forces have not been used in p-version codes, however, they can be understood as applications of the extraction procedure described in Sect. 5.1.

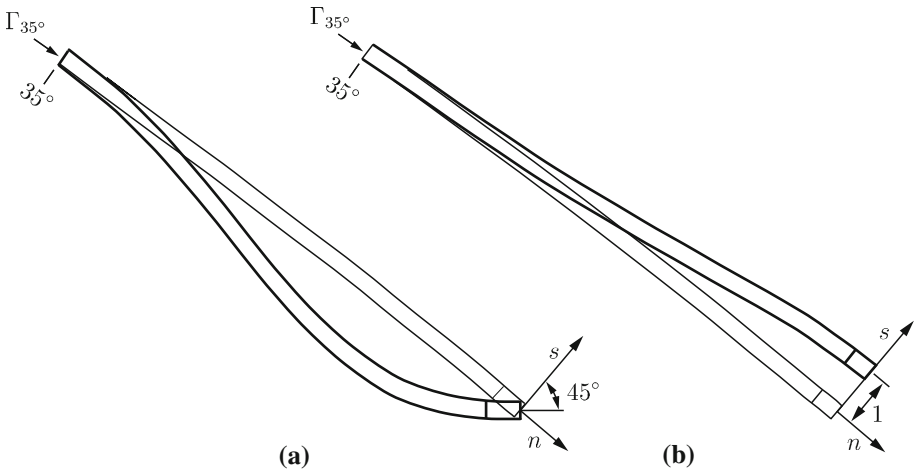

Fig. 4 Extraction functions for **a** M_α drawn to scale and **b** Q_α (not to scale)

5.2.1 The h-version

We will consider 8-node quadrilateral elements. A representative detail with generic labeling for the elements (m_1, m_2,...), nodes (n_1, n_2,...) and nodal forces is shown in Fig. 2b. The standard 8-node quadrilateral element is shown in Fig. 2c. For this element the number of *df* per field, denoted by n_f, is 8. By definition, the components of the nodal forces associated with the *k*th element are:

$$f_r^{(k,i)} = \sum_{j=1}^{2n_f} k_{ij}^{(k)} a_j^{(k)} - \bar{r}_i^{(k)} \quad i = 1, 2, \ldots, n_f \tag{31}$$

$$f_z^{(k,i-n_f)} = \sum_{j=1}^{2n_f} k_{ij}^{(k)} a_j^{(k)} - \bar{r}_i^{(k)} \quad i = n_f + 1, n_f + 2, \ldots, 2n_f \tag{32}$$

where k_{ij} are the elements of the stiffness matrix, a_j are the elements of the solution vector and $\bar{r}_i$ are the elements of the load vector corresponding to volume forces and temperature loading. The superscripts refer to the *k*th element. The superscripts on the components of the nodal force vector components f_r and f_z indicate the element number and the node numbers of the standard element shown in Fig. 2c.

Corresponding to each element k and node i associated with the standard element is a global node J which is typically shared with other elements. The nodal force vector components are summed over all elements that share node J. The resulting nodal force vector components $f_r^{(J)}$, $f_z^{(J)}$ are then treated as if they were concentrated forces when computing stress resultants. For example, in the Girkmann problem we are interested in the stress resultants Q_α and M_α. We denote the set of node numbers that lie on Γ_α by $\mathcal{N}$. The approximate values of Q_α and M_α computed from the finite element solution are:

$$Q_\alpha = \frac{1}{R_c} \sum_{J \in \mathcal{N}} (f_r^{(J)} \sin\alpha + f_z^{(J)} \cos\alpha) \tag{33}$$

$$M_\alpha = \frac{1}{R_c} \sum_{J \in \mathcal{N}} \left(-(Z_J - Z_c) f_r^{(J)} + (R_J - R_c) f_z^{(J)} \right) \tag{34}$$

where R_J, Z_J are the coordinates of the nodes that lie of Γ_α and R_c, Z_c are the coordinates of point P_0 shown in Fig. 2a.

Associated with each node is a basis function that has the value of unity in the node and is zero in all other nodes. We will denote the basis function associated with node J by $\phi_J = \phi_J(r, z)$. The basis function ϕ_J is nonzero only over those elements that share node J and it is equal to the mapped standard basis function corresponding to node J over each of those elements. We now define the vector functions $\boldsymbol{\phi}_r^{(J)} = \{\phi_J\, 0\}^T$ and $\boldsymbol{\phi}_z^{(J)} = \{0\, \phi_J\}^T$. The components of the nodal force vector in node J can be written as:

$$f_r^{(J)} = \int_{\Omega_S} \left(\mathbf{D}\boldsymbol{\phi}_r^{(J)} \right)^T \mathbf{E}\mathbf{D}\mathbf{u}_{\mathrm{FE}} r\mathrm{d}r\mathrm{d}z - \int_{\Omega_S} F_r \phi_J r\mathrm{d}r\mathrm{d}z \tag{35}$$

$$f_z^{(J)} = \int_{\Omega_S} \left(\mathbf{D}\boldsymbol{\phi}_z^{(J)} \right)^T \mathbf{E}\mathbf{D}\mathbf{u}_{\mathbf{FE}} r\mathrm{d}r\mathrm{d}z - \int_{\Omega_S} F_z \phi_J r\mathrm{d}r\mathrm{d}z. \tag{36}$$

This follows directly from the definitions of $k_{ij}^{(k)}$, $\bar{r}_i^{(k)}$, $f_r^{(J)}$ and $f_z^{(J)}$.

We select $\mathbf{w}^{(\mathbf{Q})}$ such that

$$w_s^{(Q)} = \sum_{J \in \mathcal{N}} \phi_J(r, z), \quad w_n^{(Q)} = 0. \tag{37}$$

Note that $w_s = 1$ on Γ_α and $\mathbf{w}^{(\mathbf{Q})}$ satisfies conditions similar to those given by Eq. (27) because it is zero on those edges that are opposite to the edges that lie on Γ_α. From Eq. (37) we have:

$$w_r^{(Q)} = \sum_{J \in \mathcal{N}} \phi_J(r, z) \sin\alpha, \quad w_z^{(Q)} = \sum_{J \in \mathcal{N}} \phi_J(r, z) \cos\alpha. \tag{38}$$

In view of Eqs. (33) and (35) we have:

$$Q_\alpha = \frac{1}{R_c} \left(\int_{\Omega_S} \left(\mathbf{D}\mathbf{w}^{(\mathbf{Q})} \right)^T \mathbf{E}\mathbf{D}\mathbf{u}_{FE} r\mathrm{d}r\mathrm{d}z - \int_{\Omega_S} (w_r^{(Q)} F_r + w_z^{(Q)} F_z) r\mathrm{d}r\mathrm{d}z \right). \tag{39}$$

This shows that computation of Q_α from nodal forces is formally identical to the extraction procedure, the extraction function having been constructed from the basis functions.

Similarly, we define the extraction function for M_α as follows:

$$w_s^{(M)} = 0, \quad w_n^{(M)} = -s = -\sum_{J \in \mathcal{N}} s_J \phi_J(r, z) \tag{40}$$

where s_J is the value of s in Node $J \in \mathcal{N}$. Here we assumed that the mid-side nodes are located in the mid-points of the sides. From Eq. (40):

$$w_r^{(M)} = -\sum_{J \in \mathcal{N}} s_J \phi_J(r, z) \cos\alpha,$$
$$w_z^{(M)} = \sum_{J \in \mathcal{N}} s_J \phi_J(r, z) \sin\alpha \tag{41}$$

which can be written as

$$w_r^{(M)} = -\sum_{J \in \mathcal{N}} (Z_J - Z_c) \phi_J, \quad w_z^{(M)} = \sum_{J \in \mathcal{N}} (R_J - R_c) \phi_J. \tag{42}$$

In view of Eqs. (34) and (36) we have the extraction formula for M_α corresponding to the use of nodal forces:

$$M_\alpha = \frac{1}{R_c}\left(\int_{\Omega_S} \left(\mathbf{D}\mathbf{w}^{(\mathbf{M})}\right)^T \mathbf{E}\mathbf{D}\mathbf{u}_{\mathbf{FE}} r\mathrm{d}r\mathrm{d}z - \int_{\Omega_S} (w_r^{(M)} F_r + w_z^{(M)} F_z) r\mathrm{d}r\mathrm{d}z \right) \quad (43)$$

where $\mathbf{w}^{(\mathbf{M})}$ is the extraction function for M_α, the components of which are defined by Eq. (42).

5.2.2 The p-version

We will assume that hierarchic shape functions based on Legendre polynomials are used as described in [14]. These shape functions have the important property that those shape functions which are associated with the vertices are linear, independently of the polynomial degree. Therefore the definitions given for the extraction function for Q_α in Eqs. (37)–(38) and the extraction function for M_α in Eqs. (40)–(42) are applicable to the p-version also, with the understanding that $\mathcal{N}$ is the set of vertex nodes and the mapping of the boundary where the extraction is performed is linear. Curved boundaries require special treatment which is not discussed here. In the p-version the nodal force method is equivalent to the extraction method with the domain of the extraction $\Omega_S^{\alpha,\beta}$ defined to be a single element with $\beta = 39.78°$. The results, including the number of $df\,N$ and the estimated relative error in energy norm $(e_r)_E$ on Ω, are shown in Table 1. The estimated error in energy norm was computed from the extrapolated value of the potential energy using the method described in [14]. Note that extraction over two elements yielded exactly the same stress resultants at $p = 8$, trunk space, see Sect. 5.1.

Table 1 Convergence of the shear force and bending moment computed by extraction when $\Omega_S^{\alpha,\beta}$ is a single element and $\beta = 39.78°$

p	N	$(e_r)_E$ (%)	Q_α (N/m)	M_α (Nm/m)
3	223	3.35	958.4	−39.01
4	349	1.61	946.0	−36.79
5	507	0.82	943.7	−36.89
6	697	0.64	943.6	−36.86
7	919	0.54	943.6	−36.83
8	1,173	0.46	943.6	−36.81

The 16-element mesh shown in Fig. 3 and trunk space was used

5.3 Direct computation of the stress resultants by numerical integration

The data of interest can be determined by computing the integrals defined in Eqs. (16) and (17) from the finite element solution $\mathbf{u}_{\mathbf{FE}}$ numerically. However, when $\varphi = \alpha$ then the points P_1 and P_2 shown in Figs. 2a and 5 are strongly singular which makes numerical integration difficult. The strong singularity of the stress component σ_n in the neighborhood of point P_1 is illustrated in Fig. 5a.

The results of numerical integration corresponding to the 16-element mesh are shown in Table 2. The superscripts (S) and (R) indicate, respectively, whether the integration was performed on the shell side or the ring side of Γ_α. It is seen that on the shell side the data converge strongly to values that are close to the extracted results. Much slower convergence is evident on the ring side, however. Integration was performed by Gaussian quadrature using 14 quadrature points per element side, independently of p.

The large differences between the stress resultants computed from the shell side and the ring side are indications that further investigation is necessary. In order to

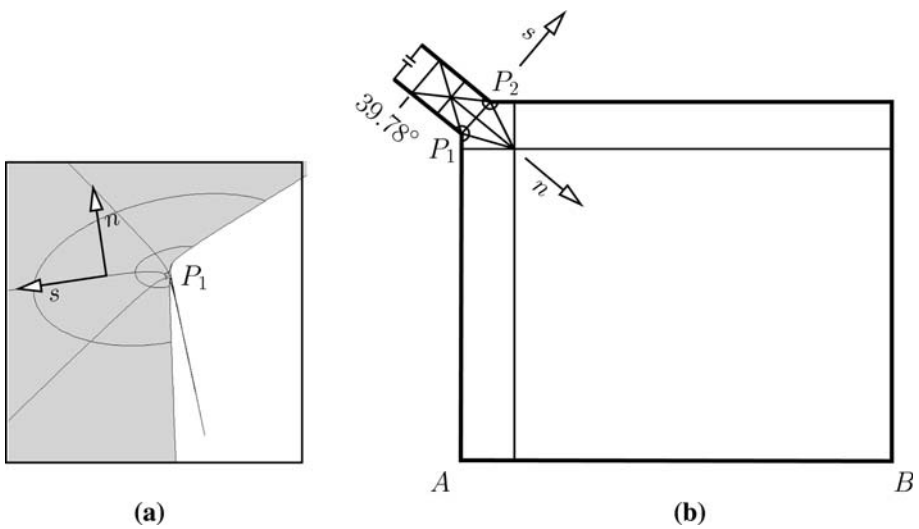

Fig. 5 **a** The stress component σ_n in the vicinity of point P_1. Perspective projection. **b** Detail of the 50-element mesh. The geometrically graded mesh at point P_1 is shown in Fig. 5a

Table 2 Convergence of the stress resultants computed by numerical integration

Discretization: 16 elements, trunk space

p	N	$(e_r)_E$ (%)	$Q_\alpha^{(S)}$ (N/m)	$Q_\alpha^{(R)}$ (N/m)	$M_\alpha^{(S)}$ (Nm/m)	$M_\alpha^{(R)}$ (Nm/m)
3	223	3.35	975.8	105.7	−38.90	6.29
4	349	1.61	946.2	389.9	−36.80	6.29
5	507	0.82	943.7	519.3	−36.89	−9.15
6	697	0.64	943.6	575.7	−36.86	−14.64
7	919	0.54	943.6	626.9	−36.83	−18.20
8	1,173	0.46	943.6	671.9	−36.81	−20.80

Table 3 Convergence of the stress resultants computed by numerical integration

Discretization: 50 elements, trunk space

p	N	$(e_r)_E$ (%)	$Q_\alpha^{(S)}$ (N/m)	$Q_\alpha^{(R)}$ (N/m)	$M_\alpha^{(S)}$ (Nm/m)	$M_\alpha^{(R)}$ (Nm/m)
3	619	3.23	2551.5	3979.3	58.72	−191.18
4	973	1.47	757.6	633.9	−34.00	−43.66
5	1,427	0.52	937.5	962.3	−37.04	−37.11
6	1,981	0.29	942.3	953.7	−37.01	−37.09
7	2,635	0.21	943.9	946.8	−36.98	−37.03
8	3,389	0.16	943.9	944.4	−36.95	−36.99

achieve satisfactory accuracy on both the ring and the shell sides, a 50-element mesh was constructed. This mesh differs from the 16-element mesh shown in Fig. 3 over the ring and the boundary layer region only which is shown in Fig. 5b. Four layers of geometrically graded elements with common factor of 0.15 in the neighborhood of point P_1, three layers in the neighborhood of point P_2 were constructed. Trunk spaces were used. The ring was assumed to be weightless, the shell was loaded by volume forces.

The results of numerical integration, including the number of *df* N and the estimated relative error in energy norm $(e_r)_E$ on Ω, are shown in Table 3. Note that at $p = 8$ the difference between M_α computed by numerical integration and by extraction (see Table 1) is less than 0.4%. Based on this and similar evidence the data reported in [5] was (conservatively) estimated to be within 2% of their exact values.

Outside of the immediate vicinity of the shell–ring interface the stress components are smooth functions. Therefore the location and magnitude of the maximum moment can be determined by numerical integration without difficulty. The bending moment as a function of the meridional angle is plotted in Fig. 6. The maximum moment occurs at $\varphi_{\max} = 38.15°$, its value is $M_{\max} = 255.1$ Nm/m.

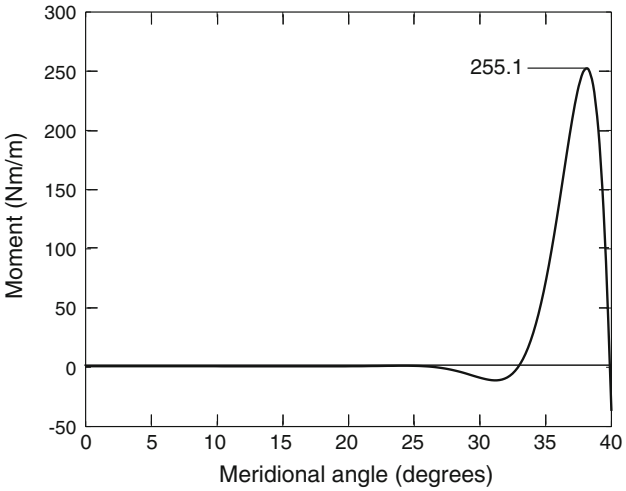

Fig. 6 Bending moment vs meridional angle

6 Results

In this section we summarize, without attribution, the results received in response to the problem statement published in [4] and reproduced here in Sect. 2. Fifteen solutions were received. All were based on the finite element method. Four solutions were based on the p-version, eleven were based on the h-version.

Respondents used various models: axisymmetric solids, axisymmetric shell–solid combinations, 3D solids and 3D shell–solid combinations. The data of interest were computed by direct integration, from nodal forces and by extraction procedures. Not all respondents included estimates of the location and magnitude of the maximum bending moment. The results are summarized in Table 4. Also shown in Table 4 are the solutions obtained by Girkmann [6] and Pitkäranta [11] by classical methods and a finite element solution published in [14]. The reasons for the significant differences between the results obtained by Girkmann and Pitkäranta are given in [11].

Table 4 Summary of results

Method	Q_α (N/m)	M_α (Nm/m)	φ_{max} (°)	M_{max} (Nm/m)
Classical—Girkmann [6]	876.6	−110.5	37.70	225.75
Classical—Pitkäranta M–B–R model [11]	942.5	−37.45	38.08	253.97
p-Version axisymmetric solid [14]	934.5	−34.81	–	–
p-Version axisymmetric solid—Extraction	943.6	−36.81	38.15	255.10
p-Version axisymmetric solid	940.9	−36.63	38.20	254.92
p-Version 3D thin solid $q = 3$—solid see Note 1	948.4	−37.31	38.20	254.50
p-Version axisymmetric solid	940.9	−36.80	38.15	254.80
h-Version axisymmetric solid—4 node elements	953.7	−10.57	–	–
h-Version axisymmetric solid—8 node elements	953.7	−19.67	–	–
h-Version axisymmetric shell—solid	593.8	−140.12	–	–
h-Version axisymmetric shel—solid	–	−78.63	–	–
h-Version 3D shell—solid	1,140.0	−205.00	37.70	215.00
h-Version 3D shell—solid	16,660.0	17,976.6	–	–
h-Version axisymmetric solid	963.2	−33.73	–	–
h-Version 3D shell—solid	1,015.7	86.30	–	231.09
h-Version axisymmetric shell—solid	949.2	−36.62	–	–
h-Version 3D shell—solid	951.3	−38.35	–	–
h-Version axisymmetric shell—solid	989.1	−89.11	38.00	238.63

The ring is assumed to be weightless. The term "thin solid, q = 3" in Table 4 is shorthand for indicating that anisotropic polynomial space was used with the polynomial degree in the transverse direction fixed at 3. For the definition of anisotropic spaces we refer to [15]

Only two of the respondents who used the h-version attempted to present evidence that verification was performed, however, the data of interest either failed to converge or appeared to have converged to the wrong result.

The results based on the p-version were well within the 5% tolerance specified in the problem statement and all respondents provided demonstration of convergence of the data of interest. On the other hand, the results based on the h-version had a very large dispersion. The reported data were within the allowed tolerance of 5% in only two of the 11 cases. These two solutions were generated by means of the same commercial finite element analysis software product and the same analyst who used (a) an axisymmetric shell–solid model and (b) a 3D solid model. This analyst did not present evidence of h-convergence, however. Other analysts who used the same software product reported results that did not meet the stated requirement.

One respondent attempted to demonstrate h-convergence for a 3D shell–solid model on one quarter of the stiffened shell using six successive mesh refinements. In the sixth refinement 120 million degrees of freedom were used. The sequence of moments corresponding to the six refinements still had not converged but appeared to tend to approximately −225 Nm/m and the shear force appeared to have converged to approximately 1,140 N/m.

Another respondent wrote *"Regarding verification tasks for structural analysis software that has adequate quality for use in our safety critical profession of structural engineering, the solution of problems such as the Girkmann problem represents a minuscule fraction of what is necessary to assure quality."* We agree with this statement. That is why we find it very surprising that the answers received had such a large dispersion. As shown in Table 4, the reported values of the moment at the shell–ring interface ranged between −205 and 17,977 Nm/m. Solution of the Girkmann problem should be a very short exercise for persons having expertise in FEA, yet many of the answers were wildly off. Analysts who cannot solve the Girkmann problem reliably are not in a position to claim that they can solve much more complicated problems reliably.

As noted in Remark 2, the ring was assumed to be weightless in references [6, 7]. This is a modeling decision most likely based on the assumption that the weight of the ring will not affect the data of interest significantly. It was found, however, that the weight of the ring accounts for approximately 10% change in M_α but the other data are insensitive to it. This effect is caused by the moment created on the ring by gravity, when the cross section of the ring is pentagonal, as in Fig. 1, rather than rectangular as assumed by Girkmann and Timoshenko.

The results of computation for a model in which the unit weight of the ring is assumed to be the same as that of the shell are shown in Table 5.

Table 5 Summary of results

Method	Q_α (N/m)	M_α (Nm/m)	$\varphi_{\max}$ (°)	$M_{\max}$ (Nm/m)
Classical—Pitkäranta M–B–R model [11]	943.8	−41.12	38.13	252.21
p-Version axisymmetric solid—nodal force	949.3	−40.91	38.20	253.94
p-Version axisymmetric solid—automesh	947.3	−40.88	38.15	253.90

The ring is assumed to have the same unit weight as the shell

7 Closing remarks

We do not have sufficient information that would enable us to explain the large dispersion of data reported in Table 4. Therefore we offer some general observations only.

As noted in Sect. 5, a prerequisite to controlling the errors of discretization is that the convergence of the sequence of discretizations in the norm appropriate for the formulation, such as the energy norm, has been proven. If the sequence of the discretized solutions does not converge in the appropriate norm then the numerical treatment is incorrect even if in some specific cases it produces credible results. This appears to have been the case when the analyst attempted a sequence of discretizations and did not observe convergence of M_α even at 120 million *df*.

Analysts who used shell–solid models tacitly assumed that the classical shell theories are applicable up to the shell–ring interface, that is over the entire range of the meridional angle $0 < \varphi < 40^\circ$. This assumption has to be justified, see Remark 5 and Fig. 5a. As part of the process of conceptualization it is necessary to determine where the interface between the shell and the solid should be, given that the data of interest are as defined in the Problem Statement. This can be decided through virtual experimentation [3].

We noted that computation of stress resultants from nodal forces was formally identical to extraction on a fixed mesh. However, in the h-version the extraction function changes as the mesh is refined and therefore we cannot speak of convergence of the extraction function in the sense of Eq. (25). Therefore it is possible that as a mesh is refined the error in the nodal forces increases faster than the error in energy norm decreases. One respondent reported lack of h-convergence in M_α but satisfactory convergence in Q_α. As far as the authors know, the accuracy of stress resultants computed from nodal forces has not been analyzed.

It is a fairly common practice to "tune" the finite element mesh so as to match some known data, such as experimental observations. This practice is ill advised because it seeks to compensate for errors in the mathematical model by errors in the numerical approximation and therefore it violates the guidelines for verification and validation. Some analysts asked what the "target values" of the data of interest were and were disappointed that we did not provide this information until the deadline for the submission of answers to the challenge problem published in [4] passed. We believe that benchmark exercises should always include the requirement of verification of the accuracy of the data of interest and an explanation of how verification was performed.

The results presented in Table 4 indicate that the requirements of verification pose challenges that users and vendors of commercial finite element analysis software products should urgently address.

Appendix: Proof of inequality (25)

The function $\mathbf{w}^{(\mathbf{M})}$ was defined on Ω_S and is extended by zero over Ω. Therefore, $\mathbf{w}^{(\mathbf{M})}$ is discontinuous on Γ_α and it does not lie in $E(\Omega)$. In other words, $\|\mathbf{w}^{(\mathbf{M})}\|_{E(\Omega)}$ has no meaning. On the other hand $\|\mathbf{w}^{(\mathbf{M})}\|_{E(\Omega_S)}$ is well defined. We define an auxiliary function $\mathbf{z}_{\mathbf{EX}}^{(\mathbf{M})} \in E(\Omega)$ as follows:

$$B_\Omega(\mathbf{z}_{\mathbf{EX}}^{(\mathbf{M})}, \mathbf{v}) = B_{\Omega_S}(\mathbf{w}^{(\mathbf{M})}, \mathbf{v}) \quad \text{for all } \mathbf{v} \in E(\Omega) \tag{44}$$

where $B_{\Omega_S}(\mathbf{w}^{(\mathbf{M})}, \mathbf{v})$ is a bounded functional on $E(\Omega)$. This guarantees that the function $\mathbf{z}_{\mathbf{EX}}^{(\mathbf{M})} \in E(\Omega)$ exists. The function $\mathbf{z}_{\mathbf{EX}}^{(\mathbf{M})}$ is uniquely determined up to rigid body displacement in the axial direction. It is continuous and smooth on Ω. By selecting $\mathbf{v} = \mathbf{u}_{\mathbf{EX}} - \mathbf{u}_{\mathbf{FE}}$, Eq. (23) can be written as:

$$M_\alpha^{(\mathrm{EX})} - M_\alpha^{(\mathrm{FE})} = \frac{1}{R_c} B_\Omega(\mathbf{u}_{\mathbf{EX}} - \mathbf{u}_{\mathbf{FE}}, \mathbf{z}_{\mathbf{EX}}^{(\mathbf{M})}). \tag{45}$$

Next we define $\mathbf{z}_{\mathbf{FE}}^{(\mathbf{M})} \in S(\Omega)$ as follows:

$$B_\Omega(\mathbf{z}_{\mathbf{FE}}^{(\mathbf{M})}, \mathbf{v}) = B_\Omega(\mathbf{z}_{\mathbf{EX}}^{(\mathbf{M})}, \mathbf{v}) \quad \text{for all } \mathbf{v} \in S(\Omega). \tag{46}$$

The function $\mathbf{z}_{\mathbf{FE}}^{(\mathbf{M})}$ is the projection of $\mathbf{z}_{\mathbf{EX}}^{(\mathbf{M})}$ onto the finite element space $S(\Omega)$. By the Galerkin orthogonality:

$$B_\Omega(\mathbf{u}_{\mathbf{EX}} - \mathbf{u}_{\mathbf{FE}}, \mathbf{v}) = 0 \quad \text{for all } \mathbf{v} \in S(\Omega) \tag{47}$$

therefore we can select $\mathbf{v} = \mathbf{z}_{\mathbf{FE}}^{(\mathbf{M})}$ and divide by R_c to obtain:

$$\frac{1}{R_c} B_\Omega(\mathbf{u}_{\mathbf{EX}} - \mathbf{u}_{\mathbf{FE}}, \mathbf{z}_{\mathbf{FE}}^{(\mathbf{M})}) = 0. \tag{48}$$

Upon subtracting Eq. (47) from Eq. (45), we have:

$$M_\alpha^{(\mathrm{EX})} - M_\alpha^{(\mathrm{FE})} = \frac{1}{R_c} B_\Omega(\mathbf{u}_{\mathbf{EX}} - \mathbf{u}_{\mathbf{FE}}, \mathbf{z}_{\mathbf{EX}}^{(\mathbf{M})} - \mathbf{z}_{\mathbf{FE}}^{(\mathbf{M})}) \tag{49}$$

and Eq. (25) follows from the Schwarz inequality.

Remark 8 Owing to the regularity of $\mathbf{z}_{\mathbf{EX}}^{(\mathbf{M})}$ on Ω the rate of convergence of $\mathbf{z}_{\mathbf{FE}}^{(\mathbf{M})}$ is likely to be comparable to the rate of convergence of $\mathbf{u}_{\mathbf{FE}}$. Therefore, the error in $M_{\alpha}^{(\mathrm{FE})}$ will be roughly proportional to the square of the error in energy norm, which is the same as the error in strain energy. Note that we have been concerned with an upper estimate of the error in $M_{\alpha}^{(\mathrm{FE})}$. Under various circumstances the actual error may be much smaller than the upper estimate. Generally speaking, the extraction method is very robust as illustrated by the numerical results presented in this paper.

References

1. AIAA Editorial Policy Statement on Numerical Accuracy and Experimental Uncertainty (1994) AIAA J 32(1):3
2. ASME V&V 10-2006 (2006) Guide for verification and validation in computational solid mechanics. The American Society of Mechanical Engineers. ISBN No. 0-7918-3042-X
3. Szabó B, Actis RL (2009) On the role of hierarchic spaces and models in verification and validation. Comput Methods Appl Mech Eng 198:1273–1280
4. Pitkäranta J, Babuška I, Szabó B (2008) The Girkmann problem. IACM Expr 22:28
5. Pitkäranta J, Babuška I, Szabó B (2009) The Problem of Verification with Reference to the Girkmann Problem. IACM Expr 24:14–15
6. Girkmann K (1956) Flächentragwerke, 4th edn. Springer, Wien
7. Timoshenko S, Woinowsky-Krieger S (1959) Theory of plates and shells, 2nd edn. McGraw-Hill, New York
8. Timoshenko S, Goodier JN (1951) Theory of elasticity, 2nd edn. McGraw-Hill, New York
9. Naghdi PM (1963) Foundations of elastic shell theory. In: Seddon IN, Hill R (eds) Progress in solid mechanics, vol 4. North-Holland, Amsterdam
10. Novozhilov VV (1964) Thin shell theory. P. Noordhoff Ltd, Groningen
11. Pitkäranta J The dome and the ring. Manuscript
12. Destuynder PA (1985) Classification of thin shell theories. Acta Appl Math 4:15–417
13. Ciarlet PG (1990) Plates and junctions in elastic multi-structures: an asymptotic analysis. RMA, vol 14. Masson, Paris
14. Szabó B, Babuška I (1991) Finite element analysis. Wiley, New York
15. Szabó B, Düster A, Rank E (2004) The p-version of the finite element method. In: Stein E, de Borst R, Hughes TJR (eds) Encyclopedia of computational mechanics, Chap, 5, vol 1. Wiley, Chichester
16. Chen Q, Babuška I (1995) Approximate optimal points for polynomial interpolation of real functions in an interval and in a triangle. Comput Methods Appl Mech Eng 128:405–417
17. Ainsworth M, Oden JT (2000) A posteriori error estimation in finite element analysis. Wiley, New York
18. Babuška I, Strouboulis T (2001) The finite element method and its reliability. Oxford University Press, Oxford
19. Babuška I, Miller A (1984) The post-processing approach in the finite element method—part 1: calculation of displacements, stresses and other higher derivatives of the displacements. Int J Numer Methods Eng 20:1085–1109